Dynamic Analysis of the Variable Stiffness Support Rotor System With Elastic Rings

Kai Sun
Northeastern University
Zhong Luo (zhluo@mail.neu.edu.cn)
Northeastern University https://orcid.org/0000-0002-0701-6123
Lei Li
Northeastern University
Jiaxi Liu
Northeastern University
Fayong Wu
Shenyang Engine Research Institute

Research Article

Keywords: Variable stiffness, Elastic ring, Mathematical model, Dynamic characteristics, Experimental verification

Posted Date: February 15th, 2022

DOI: https://doi.org/10.21203/rs.3.rs-1266032/v1

Dynamic analysis of the variable stiffness support rotor system with elastic rings

Kai Sun [a,b], Zhong Luo [a,b,c,*], Lei Li [a,b], Jiaxi Liu [a,b], Fayong Wu [d]

[a] School of Mechanical Engineering and Automation, Northeastern University, Shenyang 110819, PR China

[b] Key Laboratory of Vibration and Control of Aero-Propulsion Systems Ministry of Education of China, Northeastern University, Shenyang 110819, PR China

[c] Foshan Graduate School, Northeastern University, Foshan 528312, China

[d] AECC Shenyang Engine Research Institute, Shenyang 110015, China

[*] Corresponding author at: School of Mechanical Engineering and Automation, Northeastern University, Shenyang 110819, PR China.
E-mail address: zhluo@mail.neu.edu.cn (Z. Luo); Tel: +86 24 83680540

Abstract

Elastic rings are common rotor supporting structure, which have been widely used in aeroengine rotor-support system. However, large inertia force and gyroscopic moment may occur during the operation of aeroengine, which may lead to contact between elastic ring and bearing pedestal, and then introduce variable stiffness into the rotor-support system. In this paper, a mathematical model of variable stiffness of elastic ring is proposed and this model is subsequently verified by comparison with simulation analysis and experimental results. Based on this model, a variable stiffness model of an elastic ring-supported rotor is developed by coupling the kinetic equations of the rotor with the deformation of the combined support. Then, the spectrum cascades are used to analyze the dynamic characteristics of the rotor system. In addition, the influences of the variable stiffness of elastic ring on the critical speed of the system are also examined. Finally, some simulation results are verified by experiments on a combined test bench of an elastic ring-supported rotor.

***Keywords*:** Variable stiffness; Elastic ring; Mathematical model; Dynamic characteristics; Experimental verification.

Nomenclature

x, y	displacements in x and y directions
e	eccentricity
U_i	displacement of inner bulges
i	the ith inner bulge
n	number of inner bulges
I	moment of inertia
E	elastic modulus
L	length of the ring section
b	width of the ring
h	thickness of the ring
F_x, F_y	force of each ring segment in the x and y directions
K_1	linear segment of the elastic ring
K_2	contact stiffness of the elastic ring
ΔR	radius difference between bearing pedestal and elastic ring
$h_{\min}$	minimum wall thickness of bearing pedestal
K_{er}	variable stiffness of elastic ring
k_{b}	stiffness of bearing
k_{sq}	stiffness of squirrel cage
m_i, m_o	mass of the inner and outer race of the bearing
u^s, u^d	displacement vector of the shaft, displacement vector of the disk
$\boldsymbol{Q}^s$, $\boldsymbol{Q}^d$	excitation vector of the shaft, excitation vector of the disk
$\boldsymbol{M}_T^S$, $\boldsymbol{M}_R^S$	translating inertial matrix of beam element, rotating inertial matrix of beam element
$\boldsymbol{G}^s$, $\boldsymbol{K}_B^S$	gyroscopic moment matrix of beam element, stiffness matrix of beam element
$\boldsymbol{M}_T^d$, $\boldsymbol{M}_{d\ R}$, $\boldsymbol{G}^d$	translating inertial matrix of disk element, rotating inertial matrix of disk element, gyroscopic moment matrix of disk element
$\boldsymbol{M}^r$, $\boldsymbol{G}^r$	mass matrix of rotor substructure, gyroscopic matrix of rotor substructure
$\boldsymbol{K}^r$, $\boldsymbol{C}$	stiffness matrix of rotor substructure, damping matrix of rotor substructure
$\boldsymbol{F}_{\mathrm{e}}$, $\boldsymbol{F}_{\mathrm{b}}$, $\boldsymbol{F}_{\mathrm{g}}$	unbalance vector, bearing force vector, gravity vector
f_{n1}, f_{n2}	first and second natural frequency of the rotor system
ξ_1, ξ_2	first and second modal damping ratios
k_{B}, k_{sq}	contact stiffness of bearing, stiffness of squirrel cage
r_0, N_{b}, θ_j	bearing clearance, number of ball elements, angle location
x_r, x_o, y_r, y_o	translation of shaft and outer rings of the bearing along the x and y axes
w_{c}	angular velocity of the cage
R_{b}, r_{b}	radius of outer race, radius of inner race
n_{sq}, b_{sq}, h_{sq}, L_{sq}	number of cage strips, section width of cage strips, section height of cage strips, length of cage strips
f_{erx}, f_{ery}	elastic ring force in the x and y directions
f_{sqx}, f_{sqy}	squirrel cage force in the x and y directions
$\boldsymbol{F}_{sq}$, $\boldsymbol{F}_{\mathrm{er}}$, $\boldsymbol{F}_{\mathrm{b}}$	squirrel cage force vector, elastic ring force vector, bearing force vector

Greek symbols

Δ	height of the outer bulge
α	angle between inner and outer bulge
λ	flexibility
δ	depth of the contact
Ω	rotational speed

Abbreviations

FE	finite element
DOF	degrees of freedom
ER	elastic rings
ERSFD	elastic ring squeeze film damper

1. Introduction

Supports with elastic rings (ER) have been widely used in aero-engine rotor system [1], which are applied to adjust the rotor critical speed from the operating mode in order to reduce the vibration. To limit the deformation of elastic supports, limiting amplitude structures are set up [2]. However, the aero-engine rotor system with ER is usually exposed to great evolutionary overloading [3]. If the limited structure parameters are selected too small or the circumferential distribution is uneven, in extreme cases, due to the action of large inertia forces, the elastic supports will contact with the limiting structures, and the supporting stiffness will change, so that the system will become a rotor support system with variable stiffness [4]. Hence, in order to study the variable stiffness characteristics effectively, it's necessary to develop the combined support rotor system model with ER and analyze the dynamic characteristics of the variable stiffness rotor system.

Among the existing ER solution methods, IS [3], Artemov, Hronin and Finite element model (FE) are the most common methods to solve the stiffness [5]. However, the above methods only consider the deformation of ER within the allowable range. Thus, these methods are not suitable for the rotor with great unbalanced forces and huge weight. To limit the deformation of elastic support, Ma et al. [2] presented a novel structure with the amplitude limiting bulges. However, in extreme cases, the ER will contact the base, resulting in nonlinear stiffness of the ER. Luo et al. [6] proposed the finite element model of ER and the static stiffness test device of ER was designed based on the Guo's test [7]. Then, the characteristic of piecewise linear stiffness of ER was revealed by comparison between experiment and FE simulation. As ER exists contact stiffness，it's necessary to study contact mode. Pereira et al. [8] and Machado et al. [9] established a non-coordinated contact model of the shaft-hole with clearance. Persson et al. [10] and Ciavarella et al. [11,12] ignored the influence of hole's thickness on the contact characteristics of the shaft-hole, and established the contact force model of the shaft-hole. Li et al. [13] considered the hole's thickness and established the shaft-hole coordinated contact model. This model could provide reference for the study of contact and collision between the shaft and the hole.

From above literatures, emphasis is put on the stiffness of ER and the dynamic analysis of the rotor system is not considered. Li et al. [14,15] adopted numerical and experimental methods to analyze the dynamic properties and stability of a rotor system with bolted joint. Sun et al. [16] investigated the responses of a dual-rotor system with rub-impact, and analyzed the stability of system. Considering the influences of clearance and unbalance on rotor system, Villa et al. [17] established the rolling

bearing model with the internal clearance and Hertz nonlinearity, and presented the dynamic analysis of a rotor system with ball bearings. Hou et al. [18] analyzed the primary resonance of a dual-rotor system with ball bearings. In order to analyze the complex rotor system with combined support, Luo et al. [19] established a combined support rotor model and analyzed the dynamic response at different speeds. Chen et al. [20] proposed a novel coupling model and investigated the vibration performances of the aero-engine. In recent years, the elastic ring squeeze film damper (ERSFD), which is installed in many modern aero-engine, has been grown by many scholars. Zhang et al. [21] established a coupled oil film Reynolds equation and dynamic equation of a rotor system with ERSFD and investigated the dynamic parametric characteristics of the ERSFD. Considering the contact between the journal and the ER, Wang et al. [22,23] proposed an analytical method to investigate the dynamic properties of the ERSFD. Chen et al. [24] established the spiral bevel gear drive model with ERSFD and studied the dynamic characteristics of this system. Han et al. [25,26] proposed a semi-analytic method to analyze the oil film force of ERSFD and established a Jeffcott rotor model with ERSFD. Subsequently, this model was solved by Runge-Kutta method and the dynamic response of the ERSFD-rotor was analyzed. But there are relatively few studies on the dynamic analysis of the ER-rotor with variable stiffness [6].

Aiming at the existing issues, a variable stiffness model of ER is presented and the Newmark-β method is applied to reveal the dynamic characteristics of the variable stiffness ER-rotor system. Meanwhile, the correctness of the model is evaluated by the variable stiffness experiment of ER and some dynamic properties of ER-rotor are substantiated by numerical and experimental researches. Moreover, the research results of ER-rotor system can be a stepping stone in other rotor systems containing elastic rings.

The structure of this paper is as follows. The theoretical framework and basic idea of the variable stiffness model of ER are introduced and the kinetic equations of the ER-rotor with variable stiffness are established in Section 2. Then in Section 3, the nonlinear characteristics of rotor system caused by the ER are analyzed in detail. In Section 4, two experimental studies are illustrated to verify the ER model and some of the simulation results. Finally, the conclusions are summarized in Section 5.

2. Mathematical model and equations of motion

To conduct the dynamic investigation of a rotor system with variable stiffness elastic rings, the kinetic equations of the ER-rotor system shown in Fig. 3 are established in this section. Moreover, the variable stiffness model of elastic ring is divided into two parts according to the displacement of the

elastic ring: the linear stiffness model (Fig. 1) and the contact stiffness model (Fig. 2). Finally, according to the literature [19, 20, 27-29], the differential equations of the combined support rotor system with ER are developed.

2.1. The variable stiffness model of elastic ring

The displacement of the inner bulge of the elastic ring is related to the displacement of the rotor system. When the displacement of the inner bulge is less than the outer bulge height as shown in equation (1), the elastic ring is linear stiffness and the force analysis is shown in Fig. 1. One inner bulge is selected for analysis, and the other inner bulges are similar. F_1 represents the radial force of the inner bulge, and its components in the x and y axes are F_x and F_y, respectively. o_1 and o_2 are the centroid of ER (bearing pedestal) and journal, respectively.

$$e = \sqrt{x^2 + y^2} < \Delta \tag{1}$$

where e represents the radial displacement of the journal; x and y indicate the journal's displacement in the x and y directions; Δ is the height of the outer bulge.

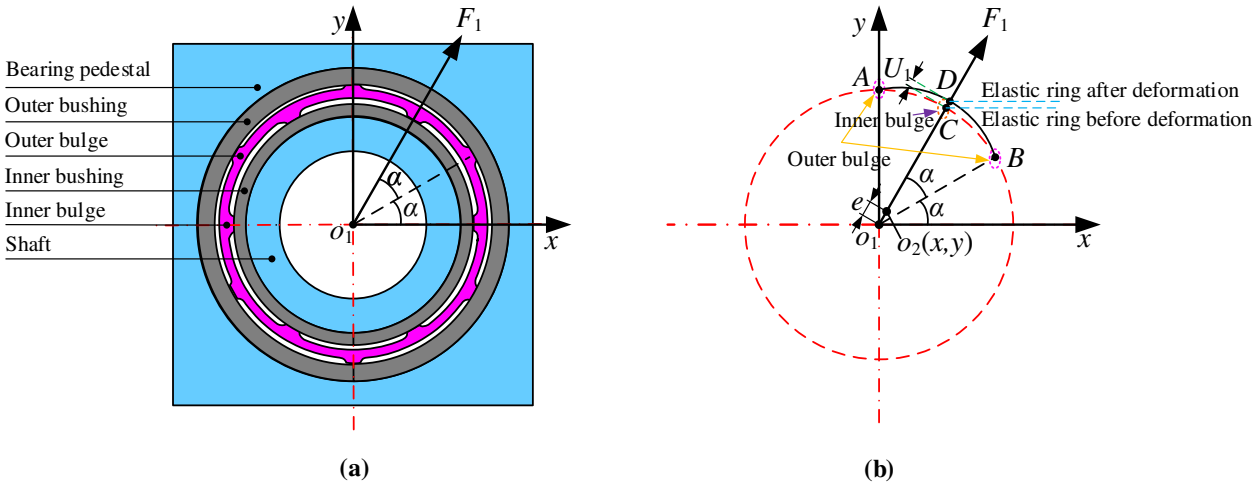

Fig. 1 Schematic of force analysis of the elastic ring with linear stiffness (a) ER model (b) detailed view

Since the inner and outer bulges of the elastic ring are in directly contact with the inner and outer bushing, it is assumed that the bulges of the elastic ring are rigid body, whose stiffness is much greater than the rest of the elastic ring [24]. The displacement of the inner bulges under the operating mode can be expressed as follows:

$$U_i = \begin{cases} x\cos(2\alpha i) + y\sin(2\alpha i) & (i = 1, 2..., n), U_i > 0 \\ 0, & \text{else} \end{cases} \tag{2}$$

where U_i represents the displacement of the inner bulges; i is the ith inner bulge and n is the number

of the inner bulges; α indicates the angle between inner and outer bulge.

The flexibility of the ring section is assumed as the flexibility at the central section of the fixed beam at both ends.

$$\lambda=\frac{L^3}{192EI} \tag{3}$$

$$I=\frac{bh}{12} \tag{4}$$

where λ represents the flexibility at the central section of the ring section; L is the length of the ring section; E is the elastic modulus of ring material; I indicates the moment of inertia of ring section; b is the width of the ring; h is the thickness of the ring.

The sum of the components of the force of each ring segment in the x and y directions are F_x and F_y, and the magnitude of the components can be expressed as:

$$\begin{cases} F_x=\sum_{i=1}^{n} F_i\cos(2\alpha i)=\sum_{i=1}^{n}\frac{U_i}{\lambda}\cos(2\alpha i) \\ F_y=\sum_{i=1}^{n} F_i\sin(2\alpha i)=\sum_{i=1}^{n}\frac{U_i}{\lambda}\sin(2\alpha i) \end{cases} \tag{5}$$

Finally, the stiffness of the linear segment of the elastic ring can be written as:

$$K_1=\frac{\sqrt{F_x^{\,2}+F_y^{\,2}}}{e} \tag{6}$$

When the displacement of the inner bulge is greater than the outer bulge height, the elastic ring is in contact with the bearing pedestal and its stiffness becomes contact stiffness. Before establishing the contact model between the elastic ring and the bearing pedestal, the following assumptions are put forward: (1) Since the height of the bulge is much smaller than the elastic ring, the bulge height is ignored. (2) The journal, inner bushing and elastic ring are approximated as shaft model. (3) The outer bushing and bearing pedestal are approximated as hole model. Then the shaft-hole contact model is introduced into the elastic ring contact model and the force analysis of the ER contact model is shown in Fig. 2. F represents the radial force, and its components in the x and y axes are F_x and F_y, respectively. o_1, o_2 and o_3 are the centroid of the bearing pedestal, the journal without contact deformation and the journal under contact deformation, respectively.

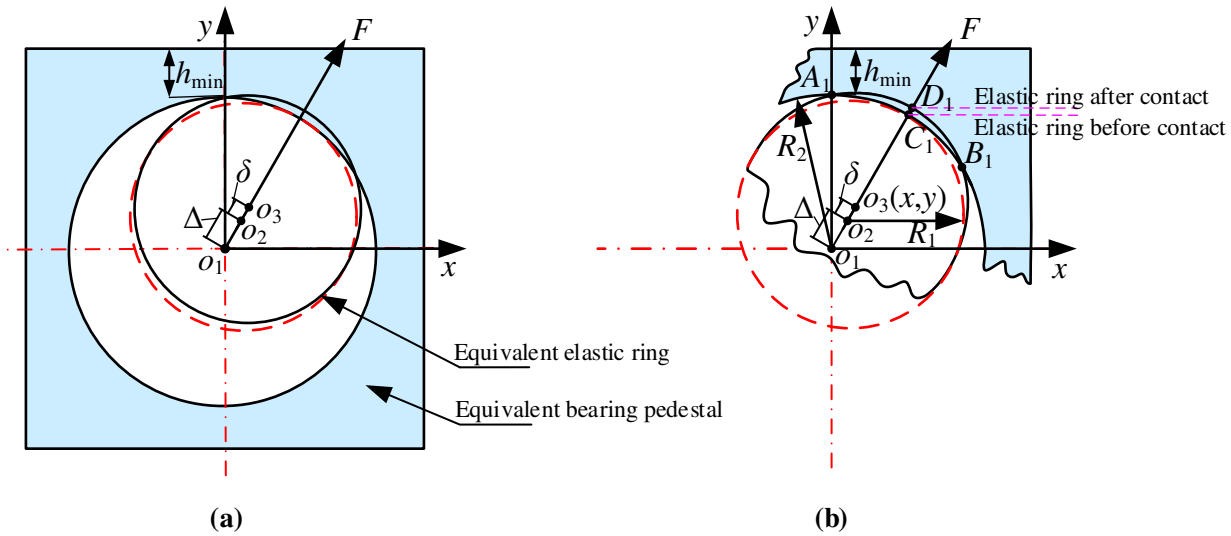

(a) (b)

Fig. 2 Schematic of force analysis of the elastic ring with contact stiffness (a) 2D contact model (b) detailed view

According to the literature [13], the nonlinear contact stiffness of the ER can be expressed as follows:

$$K_2 = \frac{4R_1E\left(\delta^2+2\delta\Delta R\right)^{\frac{3}{2}}+6R_1E\Delta R^2\left(\delta^2+2\delta\Delta R\right)^{\frac{1}{2}}}{3\left(R_1+h_{\min}\right)\left(\delta+\Delta R^2\right)} \tag{7}$$

$$\Delta R = R_2 - R_1 \tag{8}$$

$$\delta = e - \Delta \tag{9}$$

where K_2 represents the contact stiffness of the ER; R_1 is the ER radius and R_2 is the bearing pedestal radius; E is the elastic modulus of ring material; δ indicates the depth of the contact; ΔR indicates the radius difference between bearing pedestal and ER; $h_{\min}$ is the minimum wall thickness of bearing pedestal.

Then, when the displacement is greater than the height of the outer bulge, the overall force of the elastic ring can be expressed as:

$$F = K_1\Delta + \delta K_2 \tag{10}$$

The overall force's components in the x and y directions are F_x and F_y, and the magnitude of the components can be written as:

$$\begin{cases} F_x = \dfrac{xF}{\sqrt{x^2+y^2}} \\ F_y = \dfrac{yF}{\sqrt{x^2+y^2}} \end{cases} \tag{11}$$

Finally, the variable stiffness of elastic ring can be expressed as:

$$K_{er}=\begin{cases}K_1 & ,e<\Delta\\ \dfrac{(K_1\Delta+\delta K_2)}{e} & ,e\geq\Delta\end{cases} \tag{12}$$

2.2. Motion equations of the ER-rotor system

In order to analyze the rotor system with variable stiffness combined support, the rotor system is divided into rotor substructure and support substructure as shown in Fig. 3. Then, the finite element method and the lumped mass method are used to establish rotor substructure model and support substructure model respectively, where k_b, k_{sq} and k_{er} denote the stiffness of bearing, squirrel cage and ER, respectively. m_i is the mass of bearing inner race and m_o represents the mass of bearing outer race. The gyroscopic moment and rotational inertia of the shaft is considered to investigate the bending vibration of the shaft depicted in Fig. 3. Meanwhile, the rotor substructure is divided into several finite element units and each unit node has four DOFs (x, y, θ_x, θ_y).

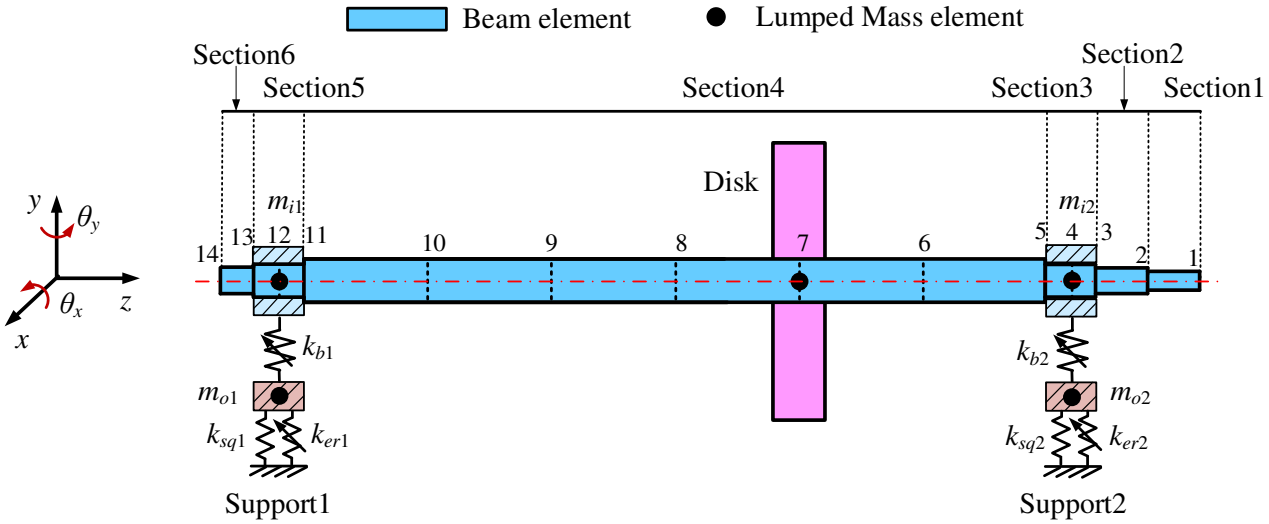

Fig. 3 Mathematical model of the rotor system with variable stiffness

The equation for the elastic shaft element is given as:

$$\left(\boldsymbol{M}_T^s+\boldsymbol{M}_R^s\right)\ddot{u}^s-\Omega\boldsymbol{G}^s\dot{u}^s+\boldsymbol{K}_B^s u^s=\boldsymbol{Q}^s \tag{13}$$

where Ω, u^s and $\boldsymbol{Q}^s$ represent the rotating speed, the displacement vector and the excitation vector of the shaft; $\boldsymbol{M}_T^s$, $\boldsymbol{M}_R^s$, $\boldsymbol{G}^s$, $\boldsymbol{K}_B^s$ are the translating inertial matrix, the rotating inertial matrix, the gyroscopic moment matrix and the stiffness matrix of the beam element, which are described in reference [29-31].

Because the disk is assumed as a rigid disk, the strain energy is ignored and only consider the kinetic energy. Then, the differential equation of the disk which is obtained by Lagrange's equations is given as:

$$\left(\boldsymbol{M}_T^d+\boldsymbol{M}_R^d\right)\ddot{u}^d-\Omega\boldsymbol{G}^d\dot{u}^d=\boldsymbol{Q}^d \tag{14}$$

where u^d and $\boldsymbol{Q}^d$ represent the displacement vector and the excitation vector of the disk; $\boldsymbol{M}_T^d$, $\boldsymbol{M}_R^d$, $\boldsymbol{G}^d$ are the translating inertial matrix, the rotating inertial matrix and the gyroscopic moment matrix of the disk element, which are given in reference [19].

Finally, the dynamic equation of the rotor substructure is obtained as follows by assembling the motion equation of the disk, the motion equation of the shaft and the supporting force.

$$\boldsymbol{M}^r\ddot{u}^r+\left(\boldsymbol{C}+\Omega\boldsymbol{G}^r\right)\dot{u}^r+\boldsymbol{K}^ru^r=\boldsymbol{F}_{\mathrm{e}}+\boldsymbol{F}_{\mathrm{b}}-\boldsymbol{F}_g \tag{15}$$

where the displacement vector u^r can be written as:

$$u^r=\left\{x_1,y_1,\theta_{x1},\theta_{y1},...,x_n,y_n,\theta_{xn},\theta_{yn}\right\} \tag{16}$$

and $\boldsymbol{M}^r$, $\boldsymbol{G}^r$, $\boldsymbol{K}^r$ and $\boldsymbol{C}$ are mass matrix, gyroscopic matrix, stiffness matrix and damping matrix of the rotor substructure; $\boldsymbol{F}_{\mathrm{e}}$ is the unbalance vector; $\boldsymbol{F}_{\mathrm{b}}$ is the bearing force; $\boldsymbol{F}_{\mathrm{g}}$ is the gravity vector and n is the number of the nodes of the rotor substructure.

The matrix of Rayleigh damping ($\boldsymbol{C}$) can be expressed as:

$$\boldsymbol{C}=\alpha\boldsymbol{M}^r+\beta\boldsymbol{K}^r \tag{17}$$

where

$$\begin{cases}\alpha=\dfrac{4\pi f_{\mathrm{n1}}f_{\mathrm{n2}}\left(\xi_1f_{\mathrm{n2}}-\xi_2f_{\mathrm{n1}}\right)}{\left(f_{\mathrm{n2}}^2-f_{\mathrm{n1}}^2\right)}\\ \beta=\dfrac{\xi_2f_{\mathrm{n2}}-\xi_1f_{\mathrm{n1}}}{\pi\left(f_{\mathrm{n2}}^2-f_{\mathrm{n1}}^2\right)}\end{cases} \tag{18}$$

where $f_{\mathrm{n1}}, f_{\mathrm{n2}}$ represent the first and second natural frequency of the rotor system and ξ_1, ξ_2 are the first and second modal damping ratios.

The combined support substructure consists of the squirrel cage, ER and the rolling bearing. Meanwhile, the supporting substructure and the rotor substructure are connected by the displacement and the interaction force of the bearing inner race and bearing outer race. Then, based on the theory of Hertz contact [32, 33], the bearing force can be expressed as:

$$\begin{aligned}f_{bx}&=k_B\sum_{j=1}^{N_{\mathrm{b}}}\left(\left(x_r-x_o\right)\cos\theta_j+\left(y_r-y_o\right)\sin\theta_j-r_0\right)^{1.5}\\&\quad\times H\left(\left(x_r-x_o\right)\cos\theta_j+\left(y_r-y_o\right)\sin\theta_j-r_0\right)\cos\theta_j\\f_{by}&=k_{\mathrm{B}}\sum_{j=1}^{N_{\mathrm{b}}}\left(\left(x_r-x_o\right)\cos\theta_j+\left(y_r-y_o\right)\sin\theta_j-r_0\right)^{1.5}\\&\quad\times H\left(\left(x_r-x_o\right)\cos\theta_j+\left(y_r-y_o\right)\sin\theta_j-r_0\right)\sin\theta_j\end{aligned} \tag{19}$$

where k_B is the contact stiffness of bearing; r_0 is the clearance of bearing; N_b is the number of ball elements; x_r, x_o, y_r, y_o are the translation of shaft and outer rings of the bearing along the x and y axes; θ_j is the angle of the jth ball, which can be expressed as [34, 35]:

$$\theta_j = \frac{2\pi(j-1)}{N_b + w_c t} \tag{20}$$

where w_c is the angular velocity of the cage, $w_c = w \times r_b/(R_b+r_b)$; R_b and r_b are the radius of bearing inner and outer race, respectively.

The nonlinear force of the ER is computed based on the variable stiffness model. It can be expressed as:

$$\begin{aligned} f_{erx} &= K_{er} x_o \\ f_{ery} &= K_{er} y_o \end{aligned} \tag{21}$$

The squirrel cage force can be expressed as [36-38]:

$$\begin{aligned} f_{sqx} &= k_{sq} x_o \\ f_{sqy} &= k_{sq} y_o \end{aligned} \tag{22}$$

$$k_{sq} = \frac{n_{sq} E b_{sq}{}^2 h_{sq}{}^2}{L_{sq}^3} \tag{23}$$

where n_{sq} is the number of cage strips; E is the elastic modulus of material; b_{sq} and h_{sq} are the width and height of cage strips, respectively; L_{sq} is the length of cage strips.

According to the coupling relationship among the squirrel cage, ER, the bearing and rotor substructure as shown in Fig. 3, the kinetic equation of the combined support rotor system can be written as:

$$\begin{bmatrix} \boldsymbol{M}^r & 0 \\ 0 & \boldsymbol{M}^o \end{bmatrix} \begin{bmatrix} \ddot{u}^r \\ \ddot{u}^o \end{bmatrix} + \begin{bmatrix} \boldsymbol{C} + \Omega \mathbf{G}^r & 0 \\ 0 & 0 \end{bmatrix} \begin{bmatrix} \dot{u}^r \\ \dot{u}^o \end{bmatrix} + \begin{bmatrix} \boldsymbol{K}^r & 0 \\ 0 & 0 \end{bmatrix} \begin{bmatrix} u^r \\ u^o \end{bmatrix} = \begin{bmatrix} \boldsymbol{F}_e + \boldsymbol{F}_b - \boldsymbol{F}_g \\ \boldsymbol{F}_{sq} + \boldsymbol{F}_{er} - \boldsymbol{F}_b \end{bmatrix} \tag{24}$$

where

$$M^o = \mathrm{diag}\left(\{m_{o1} \quad m_{o1} \quad m_{o2} \quad m_{o2}\}\right) \tag{25}$$

$$\boldsymbol{F}_{sq} = \left\{f_{sqx1}, f_{sqy1}, f_{sqx2}, f_{sqy2}\right\}^T \tag{26}$$

$$\boldsymbol{F}_{er} = \left\{f_{erx1}, f_{ery1}, f_{erx2}, f_{ery2}\right\}^T \tag{27}$$

$$\boldsymbol{F}_b = \left\{f_{bx1}, f_{by1}, f_{bx2}, f_{by2},\right\}^T \tag{28}$$

where $\boldsymbol{F}_{sq}$, $\boldsymbol{F}_{er}$ and $\boldsymbol{F}_b$ are the squirrel cage force vector, the ER force vector and the bearing force

vector of the support substructure and $\boldsymbol{F}_{sq}$, $\boldsymbol{F}_{\mathrm{er}}$ and $\boldsymbol{F}_{\mathrm{b}}$ could be acquired according from Eqs. (19) to Eqs. (23).

3. Numerical study and discussion

In this section, the linear stiffness model and the variable stiffness model of the ER are introduced into the rotor system, and the Newmark-β method is used to solve the linear and nonlinear ER-rotor system respectively. Then, by analyzing the characteristics of linear and nonlinear ER-rotor systems, the influence of variable stiffness on dynamic characteristics of ER-rotor system is illustrated. In Section 3.1, the spectrum cascades under different motor speeds of the two system are presented to illustrated the influence of variable stiffness on frequency domain characteristics. The influence of unbalance force on critical rotational speed of the variable stiffness rotor-system is illustrated by the amplitude frequency responses of the two systems under different unbalance forces. (Section 3.2). Finally, the influence of clearance on critical rotational speed of ER-rotor system is analyzed in Section 3.3.

3.1. Spectrum cascades analysis

As illustrated in Fig. 3, the combined support ER-rotor system is adopted in this section, which is modeled by using the FE method [39-42]. The ER-rotor system is divided into 6 sections, 13 beam elements of Timoshenko and 2 support elements. The Timoshenko beam element has 2 translational and 2 rotational degrees of freedom, as illustrated in Fig. 3. The dimensional parameter values of the ER-rotor system as illustrated in Fig. 3 are given in Table 1. The disk is located at node 7 and the bearings are considered as nonlinear, which are, respectively, located at node 4 and node 12. The configurations of the ball bearings are shown in Table 2. The squirrel cages are simplified as spring elements which are computed from Eqs. (23) and the configurations of the squirrel cages are shown in Table 3. The model used for ER is shown in Section 2.1 and the dimensional parameter values of the ER are given in Table 7.

Table 1 Dimensional parameter values of the ER-rotor system

Parameter	value	Parameter	value
Length of Section 1 (m)	0.025	Outer radius of Section 1 (m)	0.021
Length of Section 2 (m)	0.025	Outer radius of Section 2 (m)	0.023
Length of Section 3 (m)	0.02	Outer radius of Section 3 (m)	0.025
Length of Section 4 (m)	0.864	Outer radius of Section 4 (m)	0.028
Length of Section 5 (m)	0.02	Outer radius of Section 5 (m)	0.025
Length of Section 6 (m)	0.013	Outer radius of Section 6 (m)	0.023
m (kg) and J_p (kg.m^2) of disk	6.8943,0.0447	Inner radius of Section 1-6 (m)	0
Elastic modulus (GPa)	210	Density (kg/m^3)	7850
Shear modulus (GPa)	80	Poisson ratio of the shaft	0.3

Table 2 Configurations of the ball bearing

Parameter	value	Parameter	value
Radius of bearing outer race R_b (mm)	31	Number of bearing balls N_b	10
Radius of bearing inner race r_b (mm)	12.5	Contact stiffness k_B (N/m$^{3/2}$)	13.34×10^9

Table 3 Configurations of the squirrel cage

Parameter	value
Number of cage strips n_{sq}	10
Width of cage strips b_{sq} (mm)	3
Elastic modulus of material (GPa)	210
Length of cage strips L_{sq} (mm)	40
Height of cage strips h_{sq} (mm)	3

The ER-rotor system models with linear stiffness (the ER is simplified as a linear spring model.) and variable stiffness of ER (the ER is considered as variable stiffness model.) are established to compare the frequency domain characteristics of these two models through the spectrum cascades. In addition, the dimensional parameter values of these two models are the same. The spectrum cascades for the ER-rotor system with rotational speed, varying from 500 rev/min to 2800 rev/min, are acquired as shown in Fig. 4.

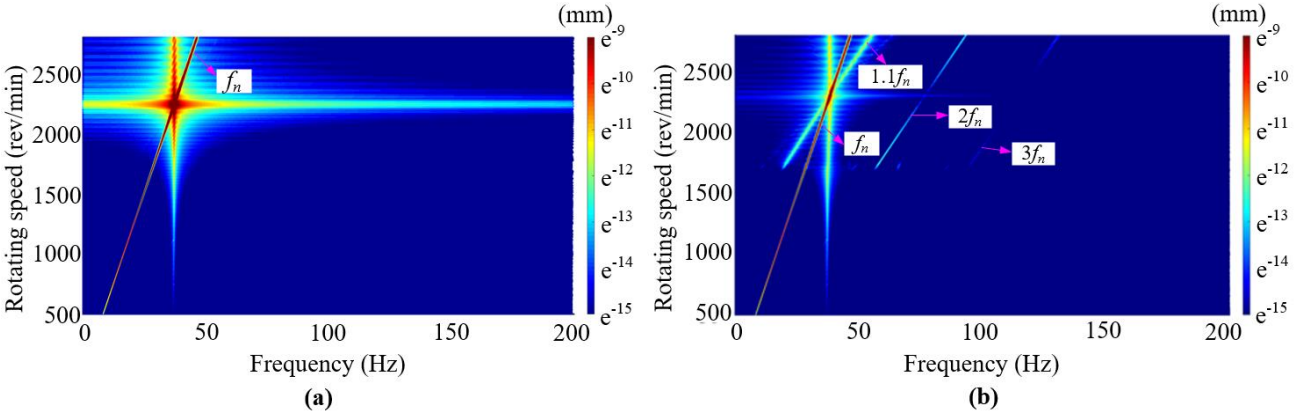

Fig. 4 Spectrum cascades of the ER-rotor system (a) the ER model with linear stiffness (b) the ER model with variable stiffness

The results from the spectrum cascades show that only the fundamental frequencies are prominent in the spectrum cascades of the model with linear stiffness (see Fig. 4a). As a contrast, for the model with variable stiffness, the spectrum cascades not only have the fundamental frequencies, but also emerge other frequency components (1.1f_n, 2f_n and 3f_n). Thus, the complex frequency components will have the significant influence on the ER-rotor system.

3.2. Influence of the unbalanced mass

In order to study the influence of the unbalanced mass on the critical speed of the ER-rotor system, in this section, the configurations of the ER-rotor system are the same except for the parameters of the unbalanced mass. The different parameter combinations of the unbalanced mass are given in Table 4. The amplitude frequency responses under four different unbalanced masses are acquired, which is shown in Fig. 5.

Table 4 Configurations of the unbalanced mass

Model	Unbalanced mass M (Kg)	Eccentric distance e (mm)
U_m1	0.0118	40
U_m2	0.0097	40
U_m3	0.0069	40
U_m4	0.002	40

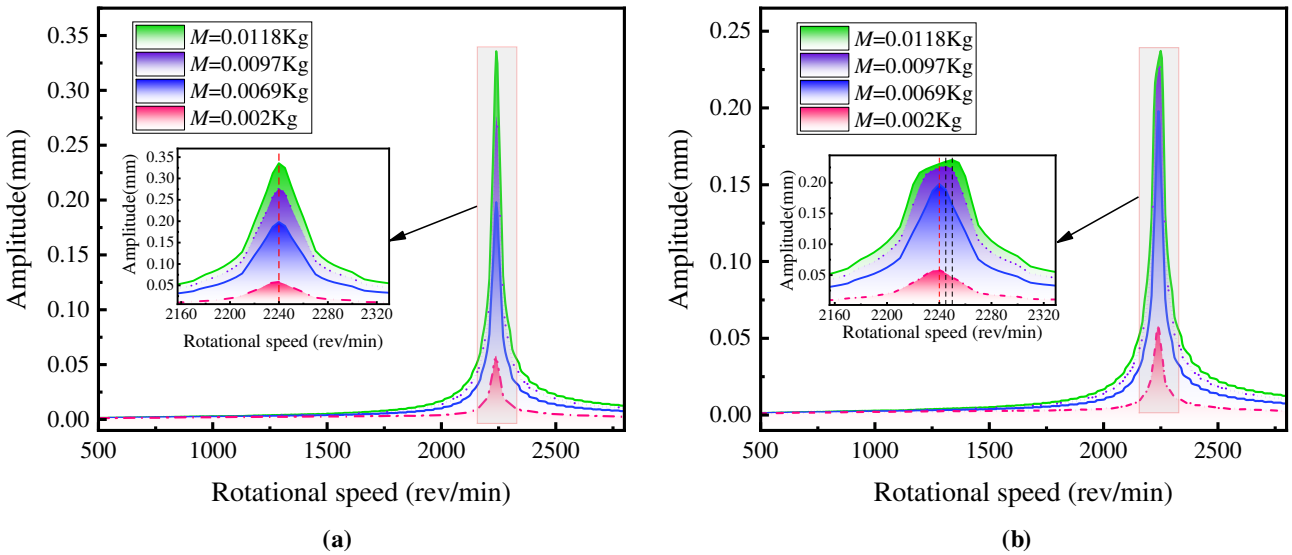

Fig. 5 Comparison of the amplitude frequency responses under four different unbalance force (a) the ER model with linear stiffness (b) the ER model with variable stiffness

Figure 5a depicts the amplitude frequency responses (the ER model with linear stiffness) corresponding to different unbalanced mass. It can be found that the first order critical speed does not change and the amplitude increases with the increase of unbalance mass. As illustrated in Fig. 5b, the amplitude frequency responses (the ER model with variable stiffness) are different from Fig. 5a. The

critical speed remains unchanged in the relatively low unbalanced mass (case3 and case4), but the relatively high unbalanced mass causes the first-order critical speed shift right (case1 and case2), which is because of the variable stiffness of the ER.

3.3. Influence of the clearance

The amplitude frequency responses for the present ER-rotor system with rotational speed (500rpm~2800rpm), are obtained as shown in Fig. 6. The configurations of the ER-rotor system are shown in Table 1-Table4. The author prefers to assigned the two parameters (M=0.0118Kg, e=40mm) directly to study the effect of different clearance on the critical speed. Meanwhile, the different parameter values of the clearance are shown in Table 5. It can be concluded that with the increase of clearance, the critical speed decreases, while the vibration amplitude increases accordingly (both Fig. 6a and Fig. 6b have the same trend).

Table 5 Parameter values of the clearance

Set No.	Clearance *clc* (mm)	Set No.	Clearance *clc* (mm)
C1	0.0525	C3	0.0175
C2	0.035	C4	0

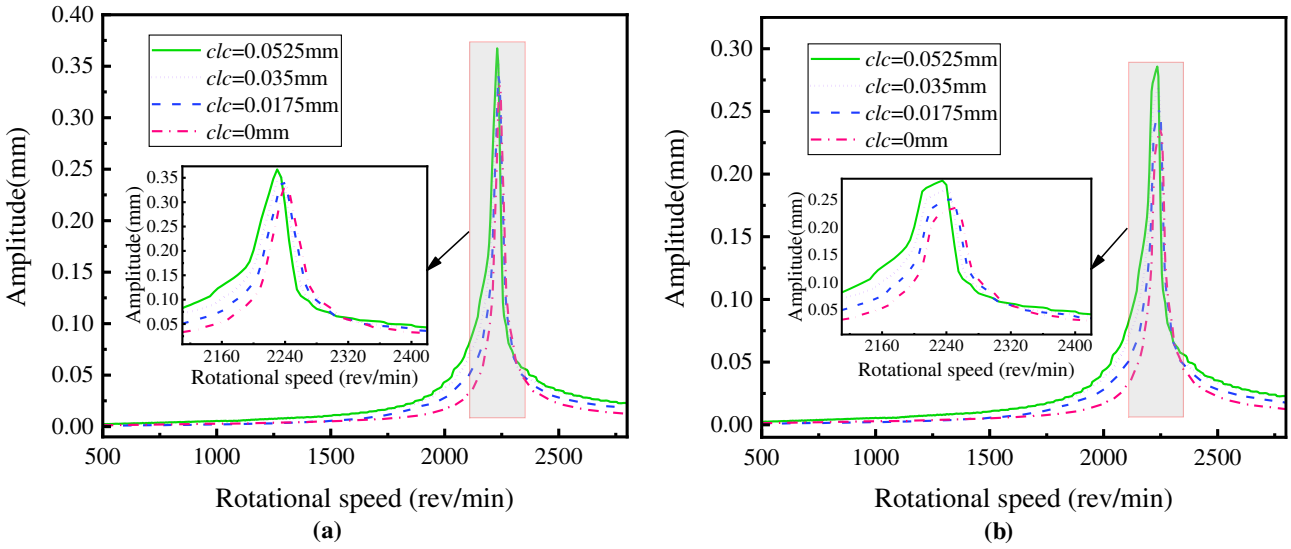

Fig. 6 Comparison of the amplitude frequency responses under different clearances (a) the ER model with linear stiffness (b) the ER model with variable stiffness

The last simulation study concerned on the influence of the unbalanced mass of the critical speed under certain clearance. Due to the existence of clearance, the stiffness of ER presents the characteristics of piecewise linear stiffness (the ER model with linear stiffness) and variable stiffness (the ER model with variable stiffness). Define clc=0.005mm and e=40mm as basic control parameters,

and the parameters of the rotor system remain unchanged. The control parameters of the unbalanced mass are given in Table. 6 and the amplitude frequency responses of the unbalanced mass under certain clearance are shown in Fig. 7. Obviously, the amplitude frequency response curves exhibit in Fig. 7 show that the clearance which is caused by design and machining will make the critical speed change. From Fig. 7a, the relatively low unbalanced mass makes the critical speed shift right, while the critical speed does not change when the unbalance mass reaches a certain degree. Different from Fig. 7a, Fig. 7b show that the clearance results in an increase of the critical speed at the relatively low unbalanced mass and the critical speed remains unchanged at the relatively high unbalanced mass. When the unbalanced mass is large, the critical speed continues to move to the right and this is due to the action of clearance and variable stiffness.

Table 6 Parameter values of the unbalanced mass under certain clearance

Set No.	Unbalance mass *M* (Kg)	Set No.	Unbalance mass *M* (Kg)
U1	0.0118	U4	0.0055
U2	0.0097	U5	0.003
U3	0.0069	U6	0.0015

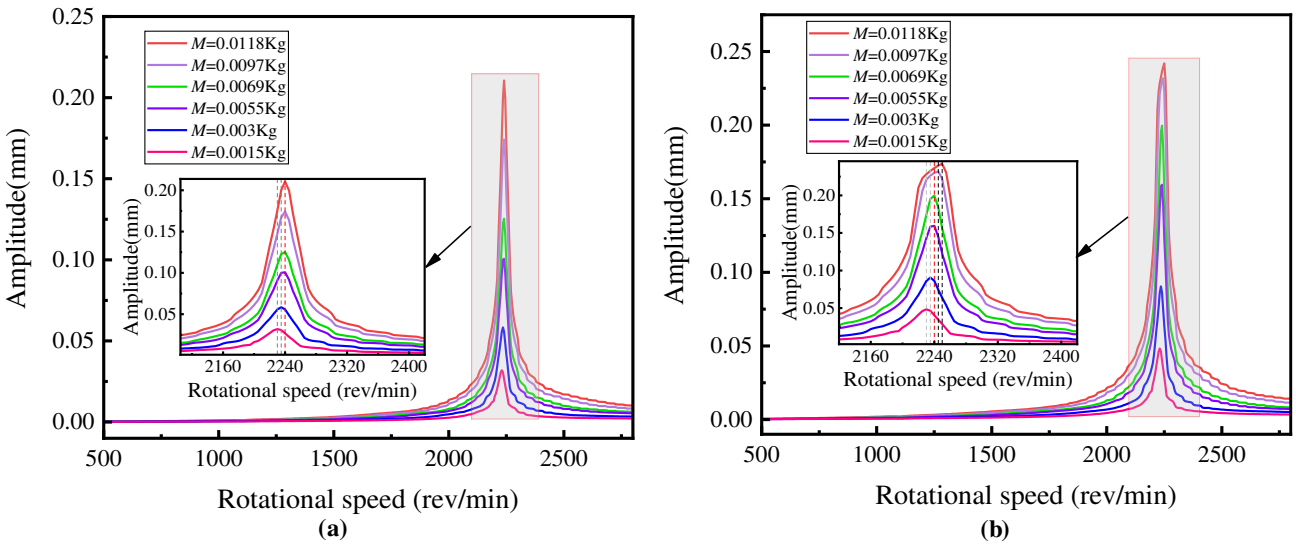

Fig. 7 Amplitude frequency responses under different unbalanced mass (a) the ER model with linear stiffness (b) the ER model with variable stiffness

4. Experimental verification

In this section, two experiments are carried out to verify the variable stiffness model of elastic ring and the partial dynamic characteristics of rotor system with elastic rings. The purpose is to demonstrate the existence and applicability of the variable stiffness model and provide guidance for the application of elastic rings in aeroengine rotor system.

4.1. Test verification of variable stiffness of elastic ring

In order to definitively prove the simulation results of the ER model with variable stiffness，the experiment about the displacement of the ER under different load has been completed on an ER stiffness test bench as shown in Fig. 8. The ER stiffness test bench consists of electro-hydraulic test machine, ER, inner and outer bushing, clamp, loading frame and rigid shaft, and more importantly, the electro-hydraulic test machine can provide the load in the vertical direction and record the displacement of the ER under the corresponding load. Then, the stiffness of ER is obtained by drawing load and displacement curves.

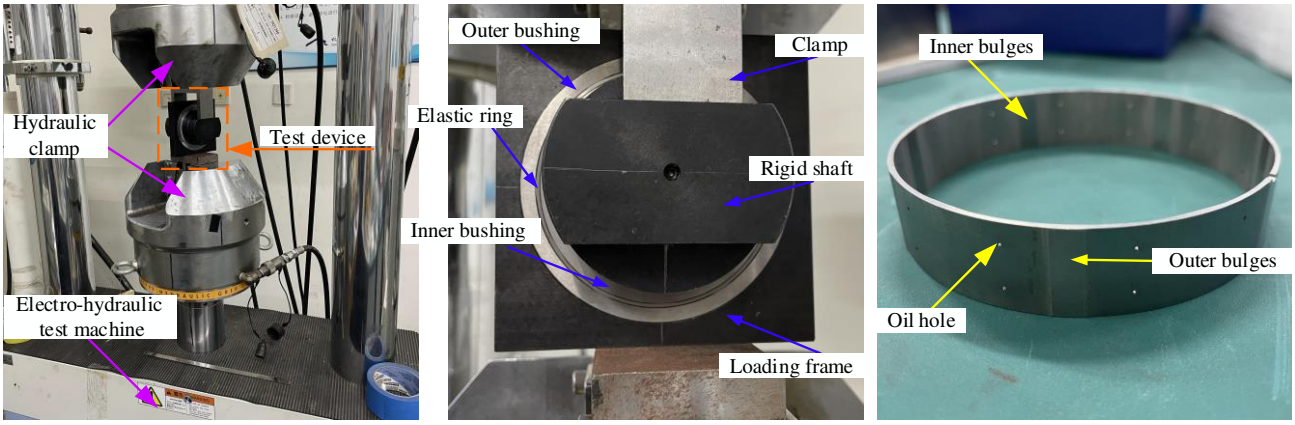

(a) **(b)** **(c)**

Fig. 8 Variable stiffness test of elastic ring (a) test equipment (b) enlarged view (c) elastic ring

In order to verify the correctness of the variable stiffness model, Table 7 summarize the parameters of the test device used in this study. Then, the stiffness of elastic ring at different circumferential positions is experimentally studied and three groups of special positions of inner bulges, holes and outer bulges are selected respectively for vertical loading, as shown in Fig. 8a, b and c.

Table 7 Parameter values of the test device

Parameter	value	Parameter	value
R_1 (mm)	40.5	R_2 (mm)	40.7
n	6	α	$\pi/6$
L (mm)	42.4	E	2×10^{11}
b (mm)	17	h (mm)	1.3
Δ (mm)	0.2	ΔR (mm)	0.2

Fig. 9 depicts the stiffness test and simulation comparison diagram of elastic ring at different circumferential positions. It is worth noting that the variable stiffness test of elastic ring has two aspects to emphasize:(1) the correctness of the variable stiffness model is verified by comparing the simulation results with the experimental results. Meanwhile when the displacement is greater than the thickness of the bulges, the elastic ring appears variable stiffness. (2) Through the comparison of test and

simulation results at different circumferential positions, it is proved that the variable stiffness model is not only suitable for a single position, but also suitable for all circumferential positions.

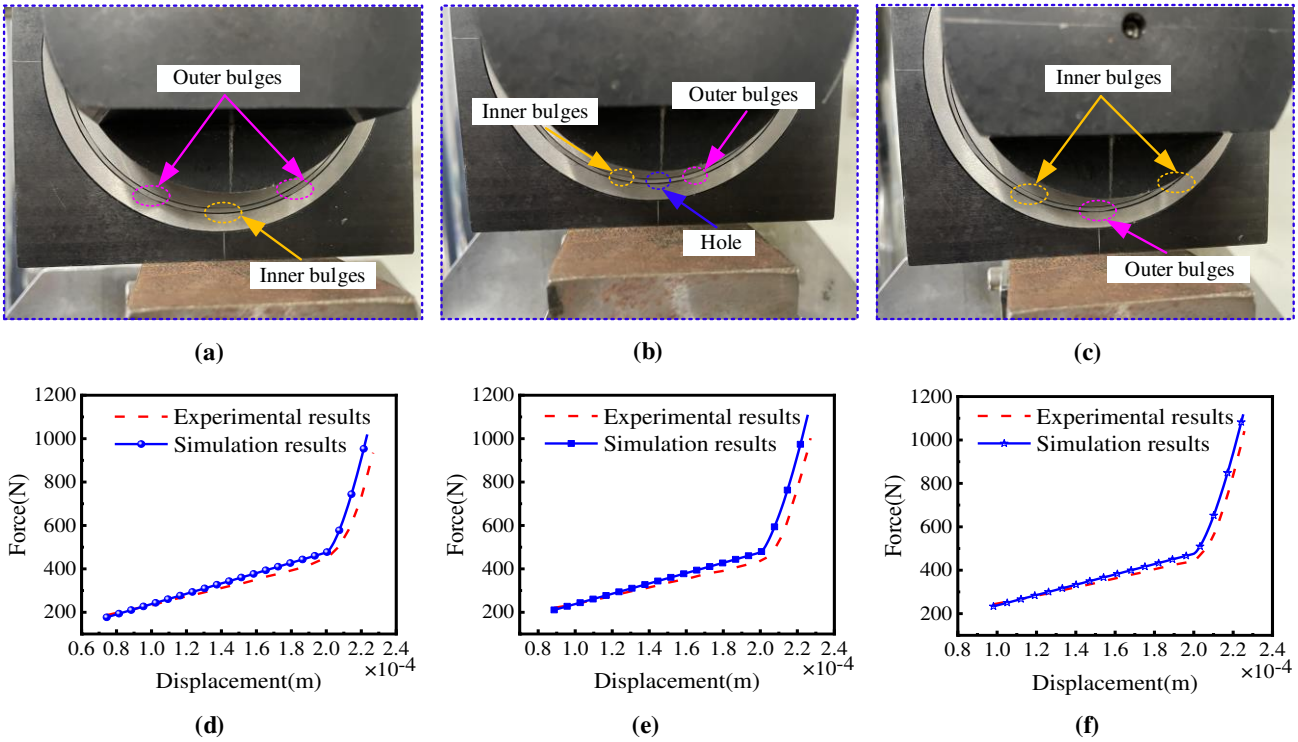

Fig. 9 Stiffness test and simulation comparison diagram of elastic ring at different circumferential positions (a) Inner bulges downward (b) Hole downward (c) Outer bulges downward (d) Inner bulges downward contrast diagram (e) Hole downward contrast diagram (f) Outer bulges downward contrast diagram

4.2. Experimental study of ER-rotor system

To verify the correctness of the simulation results for the ER-rotor system with variable stiffness, the experiment about the critical speed of the ER-rotor system under different unbalance mass has been completed on the ER-rotor test bench as shown in Fig. 10a. The ER-rotor test bench consists of a motor, disk, LMS, eddy current sensor, combined support, etc. The combined support consists of bearing, squirrel cage, and ER as shown in Fig. 10b. Meanwhile, the combined support is fixed on the bearing pedestal by bolts. The motor powers the rotor system and the rotating speed varies from 0 to 3000rpm. The combined supports at both ends of the shaft have the same configuration and the parameter values of the ER-rotor are given in Table 1, Table 2, Table 3, and Table 4. The Eddy current displacement sensors are installed on both ends of the disk and the combined support which are used to measure the displacements of the combined support and the disk. The sensitivities of the eddy current displacement sensors are 2000mV/mm and the sampling frequency is 1024Hz. The LMS is connected to the computer and the eddy current displacement sensors. Meanwhile, the displacement data of the disk

and the combined support are collected by the computer. The amplitude frequency responses curves of the ER-rotor are drawn by processing the displacements under different unbalanced masses as shown in Fig. 11. The critical speed appears near 2240 rpm, which is close to the simulation result 2260 rpm. The correctness of the ER-rotor system model is verified. As concluded in Section 3.2, the critical speed will remain unchanged with the relatively low unbalanced mass and the critical speed will shift towards right with the high unbalanced mass, this phenomenon is demonstrated in the experimental study as shown in Fig. 11.

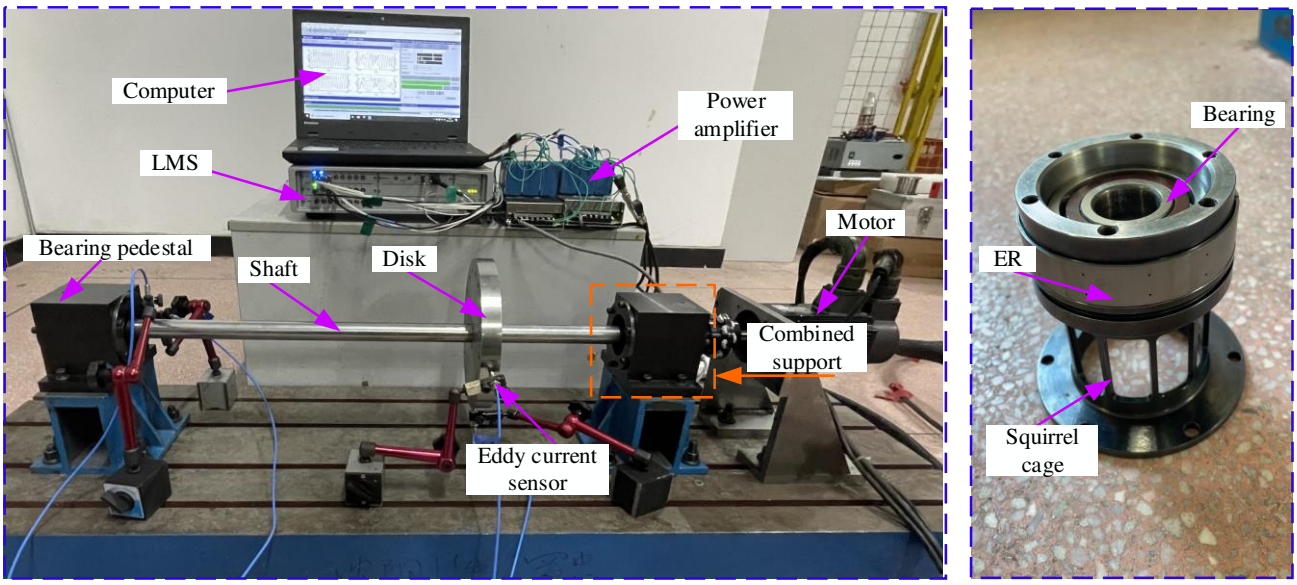

Fig. 10 (a) The ER-rotor test bench (b) The combined support

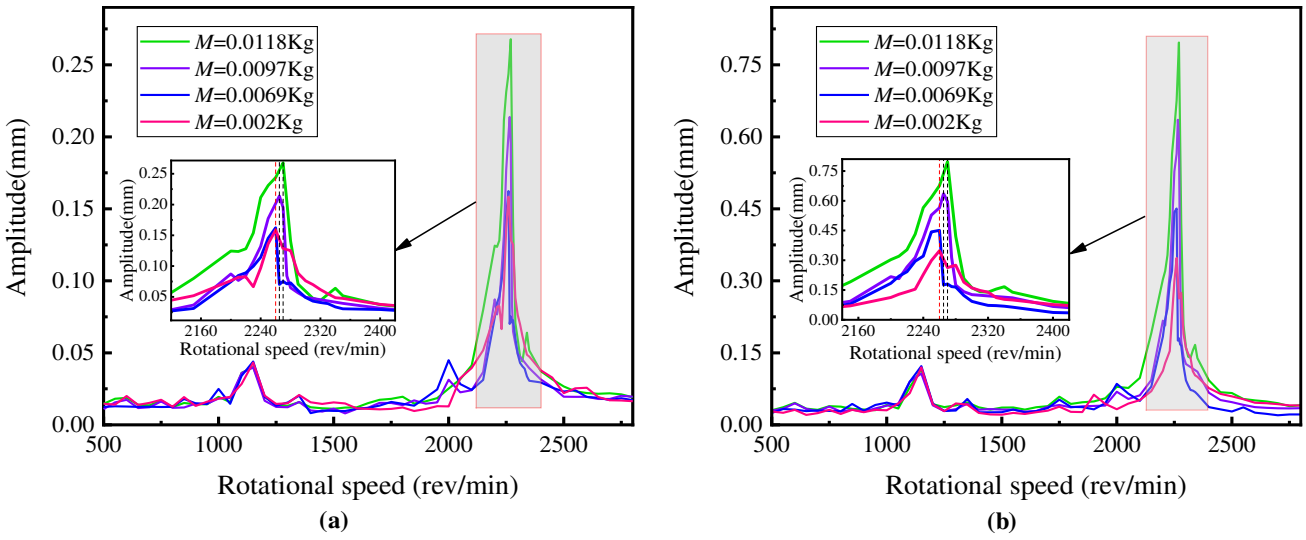

Fig. 11 Comparison of the critical speed of the ER-rotor test bench under different unbalanced mass (a) the combined support (b) the disk

It is worth mentioning that the purpose of the simulation and experimental study is to acquire

some dynamic characteristics of the variable stiffness support rotor system with elastic rings. Simulation and test results show that the variable stiffness of the ER will cause the critical speed to increase under certain conditions.

5. Conclusion

Considering that the large inertia force and gyroscopic moment may occur during the operation of aeroengine, which may lead to contact between elastic ring and bearing pedestal. This paper proposes a variable stiffness model of elastic rings and this model is subsequently verified by comparison with simulation analysis and experimental results. Meanwhile, the dynamic model of the ER-rotor is established, and the nonlinear time-varying stiffness of ER is introduced in the simulated analysis. By comparing the spectrum cascades and the amplitude frequency responses of the two ER-rotor system, the dynamic properties of the variable stiffness ER-rotor system are revealed. Finally, the correctness of the ER-rotor system model and simulation results are verified by the experimental research on the ER-rotor test bench. The conclusions are as follows:

(1) The numerical results show that only the fundamental frequencies are prominent in the ER-rotor system with linear stiffness, but the ER-rotor system produces complex frequency components ($1.1f_n$, $2f_n$ and $3f_n$) due to the variable stiffness of the elastic rings.

(2) The variable stiffness of the elastic rings has no effect on the critical speed of the rotating system at lower unbalance mass. However, due to the large unbalance mass, the displacement of the ER-rotor system increases, which leads to contact deformation of the elastic ring, and the critical speed of the ER-rotor system increases accordingly.

(3) The clearance of the elastic rings can reduce the critical speed of the system, and the critical speed of the ER-rotor system will be different with the increase of the unbalanced mass.

The research in this paper is helpful to understand the influence of variable stiffness of elastic rings on the dynamic characteristics of rotating system, and those characteristics can be used to detect the change of elastic ring stiffness in the ER-rotor system.

Conflicts of interest

The author(s) declare no potential conflicts of interest with respect to the research, authorship/contribution and publication of this original paper.

Acknowledgments

This work was supported by the National Natural Science Foundation of China [grant numbers 11872148, U1908217]; The Basic and Applied Basic Research Fund of Guangdong Province [grant numbers 2020B1515120015].

Author statement

Kai Sun: Conceptualization, Methodology, Software, Writing - Original Draft, Investigation, Validation

Zhong Luo: Writing - Review & Editing, Supervision, Formal analysis

Lei Li: Software, Validation, Visualization, Data Curation

Jiaxi Liu: Software, Visualization

Fayong Wu: Software, Visualization

Data availability statement

Data will be made available on reasonable request.

References

[1] Li, L., Luo, Z., He, F.X., Zhe, D., Sun, K.: An improved partial similitude method for dynamic characteristic of rotor systems based on Levenberg-Marquardt method. Mech. Syst. Sig. Process. **165**, 108405 (2022)

[2] Ma, Y.H., Zhu, H.X., Zhang, D.Y., Hong, J.: Experimental investigation on dynamic mechanical behavior of the elastic ring support with metal rubber. California (2013)

[3] Leontiev, M.K., Tereshko, A.G.: Research of characteristics of elastic rings mounted in rotor bearings of gas-turbine engines. (1998)

[4] Fu, C.G.: Aeroengine Manual Vol. 19. Aviation Industry Press, Beijing (2000)

[5] Diligenskiy, D.S., Novikov, D.K.: Studying of manufacturing tolerance influence on the performance of GTE rotor elastic rings. Procedia Engineering. **176**, 483-497 (2017)

[6] Luo, Z., Li, L., Yang, Y., Ding, Z.: Experimental and numerical investigations on novel models for mechanical behaviors of the elastic ring in aero-engine. Proc IMechE, Part C: J Mechanical Engineering Science. **235**(22), 6257-6267 (2021)

[7] Guo, X.M., Ma, H., Zhang, X.F., Ye, Z., Fu, Q., Liu, Z.H., Han, Q.K.: Uncertain frequency responses of clamp-pipeline systems using an interval-based method. IEEE Acess. **8**,29370 (2020)

[8] Pereira, C.M., Ramalho, A.L., Ambrósio, J.A.: A critical overview of internal and external

cylinder contact force models. Nonlinear Dyn. **63**, 681-697 (2011)

[9] Machado, M., Moreira, P., Flores, P., Lankarani, H.M.: Compliant contact force models in multibody dynamics: Evolution of the Hertz contact theory. Mech. Mach. Theory. **53**, 99-121 (2012)

[10] Persson, A.: On the stress distribution of cylindrical elastic bodies in contact. Chalmers University of Technology. (1964)

[11] Ciavarella, M., Decuzzi, P.: The state of stress induced by the plane frictionless cylindrical contact. I. The case of elastic similarity. International journal of solids and structures. **38**(26), 4507-4523 (2001)

[12] Ciavarella, M., Decuzzi, P.: The state of stress induced by the plane frictionless cylindrical contact. II. The general case (elastic dissimilarity). International journal of solids and structures. **38**(26), 4525-4533 (2001)

[13] Li, Y.T., Quan, Q.Q., Tang, D.W.: Modeling and experimental study of shaft hole coordinated contact. Journal of Harbin Engineering University. **37**(11), 1546-1552 (2016)

[14] Li, Y.Q., Luo, Z., Liu, J.X., Ma, H., Yang, D.S.: Dynamic modeling and stability analysis of a rotor-bearing system with bolted-disk joint. Mech. Syst. Signal Process. **158**, 107778 (2021)

[15] Li, Y.Q., Luo, Z., Wang, J.W., Ma, H., Yang, D.S.: Numerical and experimental analysis of the effect of eccentric phase difference in a rotor-bearing system with bolted-disk joint[J]. Nonlinear Dyn. **105**(3), 2105-2132 (2021)

[16] Sun, C., Chen, Y., Hou, L.: Steady-state response characteristics of a dual-rotor system induced by rub-impact. Nonlinear Dyn. **86**(1), 91-105 (2016)

[17] Villa, C., Sinou, J.J., Thouverez, F.: Stability and vibration analysis of a complex flexible rotor bearing system. Communications in Nonlinear Science and Numerical Simulation. **13**(4), 804-821 (2008)

[18] Hou, L., Chen, Y.S., Fu Y.Q., Chen, H.Z., Lu, Z.Y., Liu, Z.S.: Application of the HB-AFT method to the primary resonance analysis of a dual-rotor system. Nonlinear Dyn. **88**(4), 2531-2551 (2017)

[19] Luo, Z., Wang, J.W., Tang, R., Wang, D.Y.: Research on vibration performance of the nonlinear combined support-flexible rotor system. Nonlinear Dyn. **98**(1), 113-128 (2019)

[20] Chen, G.: A new rotor-ball bearing-stator coupling dynamics model for whole aero-engine

vibration. Journal of Vibration and Acoustics. **131**, 061009 (2009)

[21] Zhang, W., Ding, Q.: Elastic ring deformation and pedestal contact status analysis of elastic ring squeeze film damper. Journal of Sound and Vibration. **346**, 314-327 (2015)

[22] Wang, Z.L., Xu, N., Yu, X.Y., Liu, Z.S., Zhang, G.H.: The dynamic characteristic analysis of elastic ring squeeze film damper by fluid-structure interaction approach. Charlotte, NC, USA (2017)

[23] Wang, Z.L., Liu, Z.S., Zhang, G.H.: Dynamic characteristics of elastic ring squeeze film damper. Industrial Lubrication and Tribology. **71**(10), 1144-1151 (2019)

[24] Chen, W.T., Chen, S.Y., Hu, Z.H., Tang, J.Y., Li, H.N.: A novel dynamic model for the spiral bevel gear drive with elastic ring squeeze film dampers. Nonlinear Dyn. **98**(2), 1081-1105 (2019)

[25] Han, Z.F., Ding, Q., Zhang, W.: Dynamical analysis of an elastic ring squeeze film damper-rotor system. Mech. Mach. Theory. **131**, 406-419 (2019)

[26] Han, Z.F., Ma, Z.S., Zhang, W., Han, B.B., Ding, Q.: Dynamic analysis of an elastic ring squeeze film damper supported rotor using a semi-analytic method. Engineering Applications of Computational Fluid Mechanics. **14**(1), 1263-1278 (2020)

[27] Chen, G.: Vibration modelling and verifications for whole aero-engine. Journal of Sound and Vibration. **349**, 163-176 (2015)

[28] Li, L., Luo, Z., He, F.X., Zhao, X.Y., Liu, J.R.: A partial similitude method considering variable powers in scaling laws and applied to rotor-bearing systems. International Journal of Mechanical Sciences. **186**, 105892 (2020)

[29] Li, L., Luo, Z., He, F.X., Ding, Z., Sun, K.: A partial similitude method for vibration responses of rotor systems: Numerical and experimental verification. International Journal of Mechanical Sciences. **208**, 106696 (2021)

[30] Yang, X.D., Zhang, W., Chen L.Q., Yao, M.H.: Dynamical analysis of axially moving plate by finite difference method. Nonlinear Dyn. **67**(2), 997-1006 (2012).

[31] Liu, Y., Han, J.Y., Zhao S.Y., Meng, Q.Y., Shi, T., Ma, H.: Study on the dynamic problems of double-disk rotor system supported by deep groove ball bearing. Shock and Vibration. **2019**, 1-12 (2019)

[32] Li, B.Q., Ma, H., Yu, X., Zeng, J., Guo, X.M., Wen, B.C.: Nonlinear vibration and dynamic

stability analysis of rotor-blade system with nonlinear supports. Archive of Applied Mechanics. **89**(7), 1375-1402 (2019)

[33] Liu, Y., Xin, X.C., Zhao, Y.L., Ming, S.S., Ma, Y.X., Han, J.Y.: Study on coupling fault dynamics of sliding bearing-rotor system. Journal of Computational and Nonlinear Dynamics. **14**(4), 041005 (2019)

[34] Chen, G., Qu, M.J.: Modeling and analysis of fit clearance between rolling bearing outer ring and housing. Journal of Sound and Vibration. **438**, 419-440 (2019)

[35] Chen, G.: Study on nonlinear dynamic response of an unbalanced rotor supported on ball bearing. Journal of Vibration and Acoustics. **131**(6), 061001 (2009)

[36] Zhang, W., Han, B.B., Li, X., Sun, J.Q., Ding, Q.: Multiple-objective design optimization of squirrel cage for squeeze film damper by using cell mapping method and experimental validation. Mech. Mach. Theory. **132**, 66-79 (2019)

[37] Wang, D., Zhang, W.H., Wang, Z.P., Zhu, J.H.: Shape optimization of 3D curved slots and its application to the squirrel-cage elastic support design. Science China. Physics, Mechanics and Astronomy. **53**(10), 1895-1900 (2010)

[38] Mao, Y.Z., Wang, L.Q., Zhang, C.W.: Study on the load distribution and dynamic characteristics of a thin-walled integrated squirrel-cage supporting roller bearing. Applied Sciences. **6**(12), 415 (2016)

[39] Jin, Y.L., Lu, K., Huang, C.X., Hou, L., Chen, Y.S.: Nonlinear dynamic analysis of a complex dual rotor-bearing system based on a novel model reduction method. Applied Mathematical Modelling. **75**, 553-571 (2019)

[40] Defaye, C., Nelias, D., Leblanc, A., Bon, F.: Theoretical analysis of high-speed cylindrical roller bearing with flexible rings mounted in a squeeze film damper. Tribology transactions. **51**(6), 762-770 (2008)

[41] Qin, W.Y., Zhang, J.F., Ren, X.M.: Response and bifurcation of rotor with squeeze film damper on elastic support. Chaos, Solitons and Fractals. **39**(1), 188-195 (2009)

[42] Inayat-Hussain, J.I.: Bifurcations in the response of a flexible rotor in squeeze-film dampers with retainer springs. Chaos, Solitons and Fractals. **39**(2), 519-532 (2009)